Chinese Journal of
POLYMER SCIENCE

RESEARCH ARTICLE

https://doi.org/10.1007/s10118-026-3732-4
Chinese J. Polym. Sci.

Morphology Inversion Induced by Stimuli-responsive Blocks in the AB/BC Block Copolymer Assemblies in Solution

Zi-Xuan Zhang[a], Hao Tang[a], Xian-Deng Qiu[a], Yuan Li[b,c], Mao-Zhang Tian[b,c*], and Rong Wang[a*]

[a] *Department of Polymer Science and Engineering, State Key Laboratory of Coordination Chemistry, Key Laboratory of High Performance Polymer Materials and Technology of Ministry of Education, School of Chemistry and Chemical Engineering, Nanjing University, Nanjing 210023, China*
[b] *PetroChina Research Institute of Petroleum Exploration & Development, Beijing 100083, China*
[c] *State Key Laboratory of Enhanced Oil and Gas Recovery, Beijing 100083, China*

Electronic Supplementary Information

Abstract Co-assembly of different block copolymers has emerged as a versatile strategy for constructing stimuli-responsive polymer nanostructures with broad applications in biomedicine. However, the spatial distribution of functional blocks and the structural transition of mixed assemblies under external stimuli remain insufficiently explored, limiting the rational design of efficient delivery systems with on-demand cargo loading and release. Here, we systematically investigated the self-assembly behaviors of AB/BC mixture in solution using the dissipative particle dynamics (DPD) method. By varying the interaction parameters between different components, several classic morphologies were obtained, including vesicles (V), multicompartment vesicles (MCV), and large compound micelles (LCM). Most importantly, the distinct hydrophilic blocks (A/C) underwent microphase separation during the co-assembly process, yielding aggregates with patterns having different internal A/C distributions, such as mixed, Janus (J), and A- or C-dominated (A/C) vesicles. Upon applying external stimuli, we tracked the dynamic rearrangement process of blocks A and C, focusing on the inversion of the dominant internal block. The results revealed that kinetic factors significantly influence the inversion process, either accelerating, decelerating, or even freezing the structure. A kinetic-control mechanism for the inversion was proposed, wherein the mobility of the hydrophilic blocks and the barrier effect of the hydrophobic layer can be tuned by adjusting the interaction parameters (such as a_{BC} and a_{BS}), thereby governing the occurrence and kinetics of inversion. These findings can provide valuable insights into the precise modulation of block distribution and rearrangement in stimuli-responsive aggregates, offering applications in controlled drug delivery and release processes.

Keywords Co-assembly; Diblock copolymer mixture; Dissipative particle dynamics; Inversion mechanism

Citation: Zhang, Z. X.; Tang, H.; Qiu, X. D.; Li, Y.; Tian, M. Z.; Wang, R. Morphology inversion induced by stimuli-responsive blocks in the AB/BC block copolymer assemblies in solution. *Chinese J. Polym. Sci.* https://doi.org/10.1007/s10118-026-3732-4

INTRODUCTION

The self-assembly of block copolymers (BCPs) driven by non-covalent interactions (*e.g.*, hydrophobic, van der Waals, electrostatic, and hydrogen bonding) enables the formation of nanostructures with diverse morphologies and complex architectures.[1–4] These materials hold significant potential across a range of fields, such as biomedicine,[5–7] energy storage and conversion,[8] and microelectronics.[9] In recent years, growing functional demands have imposed higher requirements on the compositional and geometric complexity of self-assembled nanostructures, exceeding the capabilities of conventional systems like AB diblock copolymers. While designing block copolymers with intricate topologies and novel components presents one solution, challenges, such as complex assembly pathways, limited structural control, and high synthesis costs, hinder their practical application. To overcome these limitations, co-assembly of block copolymer mixtures has emerged as a promising alternative strategy to construct functionally integrated and hierarchically organized polymer nanostructures.[10,11] This approach provides a pathway to introduce a second level of hierarchy, offering advantages such as enhanced aggregate stability, simple synthesis, and easier integration of functional building blocks.[12] Currently, co-assembly strategies based on block copolymer mixtures have been widely employed in fields such as nanomedicine[12–14] and synthetic membranes.[15–17] Especially in biomedical applications, the mixing strategy enables improved drug loading, tighter size control, and the incorporation of multiple functionalities (*e.g.*, pH sensitivity, temperature responsiveness, and targeting ligands),[18–20] facilitating targeted delivery and controlled release of therapeutic payloads. Various mixed systems have been developed for use in drug therapy,[21] gene delivery,[22] and bioimaging.[23]

By employing co-assembly strategies and systematically adjusting factors such as block composition and solvent

* Corresponding authors, E-mail: mztian@petrochina.com.cn (M.Z.T.)
E-mail: wangrong@nju.edu.cn (R.W.)
Received February 28, 2026; Accepted April 29, 2026; Published online June 26, 2026

properties, nanoparticles with diverse morphologies and complex internal structures can be fabricated, including disk-spheres,[24] disk-cylinders,[24] pupa-like multicompartment micelles,[25] complex coacervate core micelles,[26] and spotted vesicles.[27] Additionally, various auxiliary techniques are also employed to modify interactions between blocks, such as hydrogen bonding,[28] small-molecule/ion additives,[24,27] and homopolymer complexation.[29] The synergistic behavior of block copolymers in mixed systems holds great promise for generating novel structures with unique functionalities. Consequently, co-assembly mechanisms have attracted considerable research interest.[30–33] Compared to experimental methods, computational simulations provide an opportunity to explore a broad range of parameter spaces and extended time scales.[34–38] For instance, Wang et al. used dissipative particle dynamics (DPD) to construct multi-geometry nanoparticles via the co-assembly of diblock copolymer blends, achieving hybrid core/shell geometries by tuning the relative chain lengths and volume fractions.[39]

In copolymer mixtures, self-assembly is typically driven by weak interactions with blocks that often contain stimulus-sensitive segments. As a result, aggregates may undergo structural transitions and segment rearrangements in response to external stimuli, exhibiting dynamic and tunable properties.[40,41] This characteristic holds significant research value for enhancing controlled encapsulation and triggered drug release, and has been used to develop stimulus-responsive drug delivery vehicles where drug release could be triggered by endogenous or exogenous activation.[42,43] However, the distribution of functionalized blocks within aggregates formed through co-assembly remains insufficiently explored. The factors influencing structural transitions and underlying regulatory mechanisms remain unclear, limiting the development of advanced smart polymeric assemblies for medical and biological applications.

In this work, we employed the DPD method to investigate the co-assembly behavior of the binary AB/BC diblock copolymer mixture in solution. By systematically varying the interaction parameters, we examined their influence on the morphology of the mixed assemblies and obtained several structures with different internal distributions of hydrophilic blocks A and C. Subsequently, we tracked the dynamic rearrangement of the hydrophilic blocks induced by changes in the interaction conditions and investigated the mechanism governing the inversion of the dominant internal block. This work is expected to provide valuable insights for the design of novel drug vehicles tailored to meet functional requirements and specific applications.

METHOD AND MODEL

In this work, the DPD method was used to investigate the co-assembly behavior of the mixed BCP system. DPD is a mesoscopic coarse-grained simulation method extensively applied to study the behavior of complex fluids due to its time-space scale and satisfactory computational efficiency.[44–46] More details about the DPD method can be found in Part I of the electronic supplemetary information (ESI).

The simulation system consists of two different diblock copolymers (AB/BC) that possess the same hydrophobic blocks, so there are four different types of DPD beads: hydrophilic beads (A/C), hydrophobic beads (B), and solvent beads (S) in the simulation system. Each diblock copolymer chain consists of 13 DPD beads, and the A_4B_9/B_9C_4 mixture was chosen to yield well-formed vesicles, as indicated by the results in Figs. S1 and S2 (in ESI). The ratio of AB to BC is fixed at 1:1. In the DPD simulations, the interaction cutoff radius r_c, the bead mass m, and the thermostat temperature k_BT are selected as reduced units. We carry out the simulations in a cubic box ($V = 30^3$) under periodic boundary conditions with the number density $\rho = 3$. The friction coefficient γ and the noise amplitude σ are set to 4.5 and 3.0, respectively. Each simulation is performed at least $2\times10^6\Delta t$ to ensure equilibration, where the time step Δt is set to 0.03τ ($\tau = \left(mr_c^2/k_BT\right)^{1/2}$). The pairwise repulsive interaction parameter between DPD beads of the same type is set to $a_{ii} = 25$, whereas the interaction parameter a_{ij} between i- and j-type beads can be estimated from the Flory-Huggins interaction parameter χ_{ij} by $a_{ij} = a_{ii} + 3.27\chi_{ij}$.[47] All simulations are carried out using the parallel simulation package LAMMPS,[48] and the software OVITO[49] is used for visualization.

RESULTS AND DISCUSSION

In general, the co-assembly of AB/BC diblock copolymers is influenced by a large parameter space, such as the chain lengths of the hydrophilic blocks, mixing ratio of the two BCPs, and interaction between the solution and BCPs.[32,50,51] In this work, we primarily focus on the effects of interaction parameters (a_{ij}) on the morphology and internal structure of the mixed aggregates. Subsequently, we simulate the change in block properties triggered by external stimuli through dynamic adjustments of a_{ij} and investigate the mechanism governing the structural transition of the aggregates.

By varying the interaction parameters between different components, several classic morphologies are obtained, including vesicles (V), multicompartment vesicles (MCV), and large compound micelles (LCM). Microphase separation occurs both on the outer surface and within the aggregates due to the incompatibility between the two different hydrophilic blocks. The contact between the surface A and C blocks increases the repulsion outside the vesicle, which contributes to maintaining the vesicle curvature.[52] The confined internal space of the aggregates further promotes microphase separation. Therefore, based on the spatial distribution of the two types of hydrophilic blocks within the aggregates, the above morphologies can be subdivided into several types of patterned vesicles: mixed, Janus (J), and A- or C-dominated (A/C), as shown in Fig. 1(a). The distribution and microphase separation of hydrophilic blocks within the aggregates can be further identified by the radial distribution of blocks A and C and the corresponding snapshots of A-V and C-V morphologies, as shown in Figs. 1(b) and 1(c). The typical process of vesicle formation in the AB/BC mixture follows the bilayer membrane closure mechanism (Fig. S3 in ESI).

Effect of Interaction Parameters on Co-assembly Morphology of Patterned Vesicles

Here, we simulate the effect of interactions between different components on the co-assembly morphology by tuning the in-

teraction parameters. Fig. 2(a) shows the morphological phase diagram of the aggregates formed by the A_4B_9/B_9C_4 diblock copolymer mixture by systematically varying a_{AC} and a_{CS}. As the repulsive interaction between block C and the solvent increases, the aggregates generally transition from vesicles to multi-compartment vesicles. Moreover, block C gradually dominates the inner region, indicating that the enhanced incompatibility between the hydrophilic block and solvent promotes its preferential distribution inside the aggregates. This is because more hydrophilic blocks are more extensively stretched in the selective solvent, tending to accumulate on the outer layer of the aggregates, where the spatial volume is larger. This increases contact with the solvent, thereby facilitating a reduction in the system's energy. a_{AC} reflects the incompatibility between blocks A and C, and as a_{AC} increases, progressively stronger repulsive interactions between A and C blocks drive the microphase separation. When a_{AC} reaches a sufficiently high value ($a_{AC} > 70$), the interior of the aggregate is almost entirely composed of either A or C blocks, resulting in A-V and C-V morphologies. It is observed that when properties of blocks A and C are set to be identical ($a_{AB} = a_{BC} = 50$, $a_{AS} = a_{CS} = 26$) and the repulsive interaction between A and C is sufficiently strong ($a_{AC} \geq 100$), vesicles with an inner surface composed of either A or C blocks form with equal probability, corresponding to the A/C-V region of the phase dia-

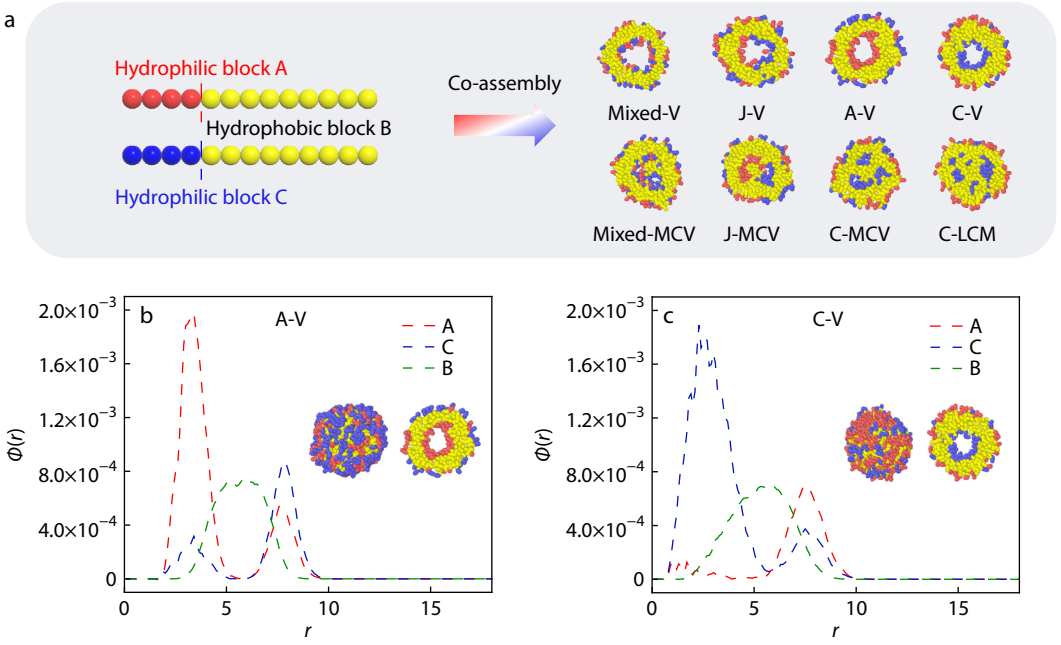

Fig. 1 (a) Schematic model of the two co-assembled block copolymers AB/BC and cross-sectional slices of different patterned structures formed by the mixture: mixed/Janus/A-dominated/C-dominated vesicles (mixed-V/J-V/A-V/C-V), mixed/Janus/C-dominated multicompartment vesicles (mixed-MCV/J-MCV/C-MCV), and C-dominated large compound micelles (C-LCM). The red and blue beads represent hydrophilic blocks A and C, respectively, while the hydrophobic blocks B are shown in yellow. The normalized radial distribution functions ($4\pi \int \Phi(r) r^2 dr = 1$) of hydrophilic A beads $\Phi_A(r)$, hydrophilic C beads $\Phi_C(r)$, and hydrophobic B beads $\Phi_B(r)$ as a function of the distance r from the geometric center of the vesicles: (b) A-V ($a_{AB}=a_{BC}=a_{AC}=70$, $a_{AS}=30$, $a_{CS}=26$, $a_{BS}=80$) and (c) C-V ($a_{AB}=a_{BC}=50$, $a_{AC}=100$, $a_{AS}=26$, $a_{CS}=27$, $a_{BS}=80$), with polymer concentration $\varphi=0.10$. The insets show the corresponding snapshots and cross-sectional slices of the vesicles.

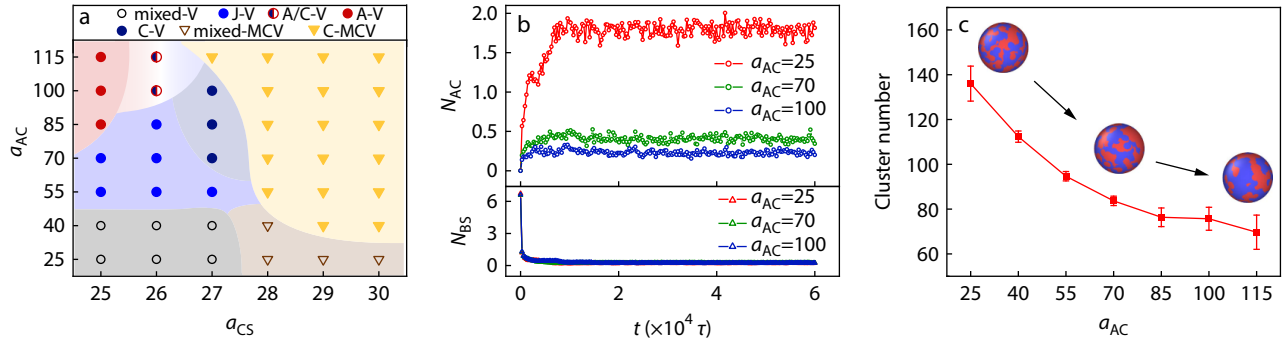

Fig. 2 (a) Morphological phase diagram of the co-assembled aggregates formed by A_4B_9/B_9C_4 diblock copolymer mixture in terms of the interaction parameters a_{AC} and a_{CS} with fixed parameters: $a_{AB}=a_{BC}=50$, $a_{AS}=26$, $a_{BS}=80$, and $\varphi=0.10$. (b) Time evolution of the contact numbers, N_{AC} and N_{BS}, with $a_{CS}=26$ and $a_{AC}=25/70/100$. (c) Number of A clusters plus C clusters as a function of a_{AC} when $a_{CS}=26$. The insets represent the snapshots of the patterned vesicles rendered by projection on spherical surface.

https://doi.org/10.1007/s10118-026-3732-4

gram.

To quantitatively characterize the microphase separation process between blocks A and C, we first analyzed the time evolution of the contact numbers (N) between block B and solvent S (N_{BS}), and between blocks A and C (N_{AC}). As shown in Fig. 2(b), N_{BS} drops rapidly at the beginning, indicating the fast aggregation of the hydrophobic B blocks in the solvent, which reduces the unfavorable interaction enthalpy with the solvent and leads to the formation of the hydrophobic membrane, and then N_{BS} remains mostly unchanged until the end of the simulation. A similar N_{BS} evolution trend is observed at different values of a_{AC} (= 25, 70, and 100), suggesting that the overall aggregation degree is comparable. Meanwhile, N_{AC} increases significantly with time and reaches a steady plateau after approximately $1.5\times10^4\tau$, indicating that the system has reached equilibrium. Notably, a higher a_{AC} results in a lower N_{AC}, reflecting the enhanced microphase separation. To further quantify this effect, we also calculated the number of A and C clusters at different values of a_{AC}, as shown in Fig. 2(c). With increasing repulsive interactions between blocks A and C, the total number of A and C clusters decreases, indicating an increase in the average cluster size and a higher degree of segregation between the two blocks. The insets in Fig. 2(c) display snapshots of the vesicle rendered by projection onto a spherical surface, providing direct visual evidence of enhanced microphase separation. Based on these results, a_{AC}= 70 was chosen for subsequent simulations to maintain moderate, yet well-defined repulsive interaction between blocks A and C.

Next, we investigated the effects of a_{BC} and a_{BS} on the co-assembled morphologies, as shown in Fig. 3. When the repulsive interaction between blocks B and C is weak, multicompartment assemblies (*e.g.*, C-MCV and C-LCM) are observed. This behavior is closely related to the dynamic process of aggregate formation. During the early stage collision and fusion of small micelles, the weak repulsion between blocks B and C facilitates the incorporation of C blocks into the interior of the fused micelles. Continued fusion of these micelles ultimately leads to the formation of multi-compartment structures with internal C blocks. Increasing a_{BC} promotes the formation of vesicular structures. With increasing a_{BC}, the repulsive interaction favors the formation of disk-like micelles, which subsequently bend and close to form vesicles. It is observed that as a_{BC} further increases, the fraction of C blocks distributed on the inner surface decreases, resulting in a morphology transition from J-V to A-V. This trend can be attributed to the confined interior of the vesicles, where spatial restriction enhances unfavorable contacts between the hydrophilic and hydrophobic blocks. To minimize the system's energy, blocks that are more incompatible with block B are disfavored on the inner surface. As a result, C blocks show a preferential distribution on the outer surface of the vesicles at higher a_{BC}. The parameter a_{BS} mainly affects the compactness of the hydrophobic membrane. Weaker repulsion between the hydrophobic block and the solvent (a_{BS}=50) produces a loosely packed vesicle structure, accompanied by incomplete microphase separation and the formation of mixed-V structures.

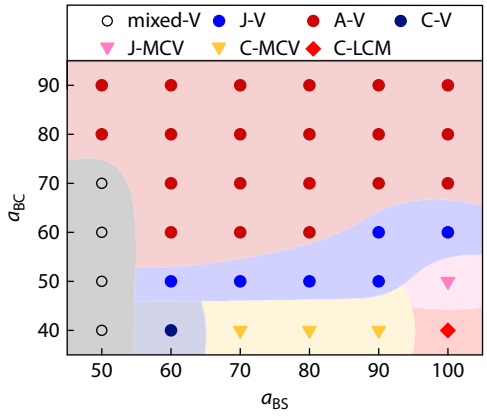

Fig. 3 Morphological phase diagram of the co-assembled aggregates in terms of the interaction parameters a_{BS} and a_{BC} when a_{AC} = 70, a_{AB} = 50, a_{AS} = 26, a_{CS} = 26 and φ = 0.10.

The above results systematically present the effects of the interaction parameters on the aggregation morphology formed by the A_4B_9/B_9C_4 mixture. To introduce distinct properties between blocks A and C, in the following simulation cases, we set the interaction parameters a_{AS}=30 to endow block A with weak hydrophilicity to facilitate subsequent adjustment of a_{CS} while maintaining the stability of the aggregates, and a_{AB}=70 and a_{BC}=50 to introduce property differences between blocks A and C. Moreover, a_{BS}=80 was set to endow block B with strong hydrophobicity.

Morphology Inversion Induced by External Stimuli

External stimuli (*e.g.*, pH and temperature) can alter the physicochemical properties of the stimuli-sensitive blocks, thereby inducing structural transitions in the aggregates. By exploiting this responsiveness, various stimuli-responsive block copolymer assemblies have been developed as drug carriers, enabling precise spatiotemporal control over drug delivery.[53] From the investigations presented above, aggregates exhibiting distinct internal distributions of hydrophilic blocks were observed. These observations raise a key question: can external stimuli induce inversion of the dominant internal block? To address this question, we investigate the inversion process and the underlying mechanisms governing the arrangement of the hydrophilic blocks.

To investigate the effect of polymer concentration (φ) and the hydrophilicity of block C (a_{CS}) on the aggregation morphology, we constructed a morphological phase diagram shown in Fig. 4(a). Based on the phase diagram, φ=0.06 was selected for subsequent studies to enhance intra-aggregate phase separation. The hydrophilicity of block C was tuned by varying the interaction parameter a_{CS} from 26 to 36, which mimicked the response of the block copolymer mixture to external stimuli. According to the phase diagram, representative morphologies with distinct internal distributions of the hydrophilic blocks were identified. When a_{CS}=26, A blocks predominantly occupy the inner surface of the vesicles (A-V). With increasing a_{CS}, the enthalpy penalty of interaction between the hydrophilic C blocks and the solvent rises, driving block C to preferentially localize within the aggregates (C-LCM). It should be noted that, strictly speaking, the aggregates formed at higher a_{CS} do not correspond to the genuine C-LCM structure. At the low polymer concentration of φ=0.06, the C blocks assemble into a single cluster within the aggre-

https://doi.org/10.1007/s10118-026-3732-4

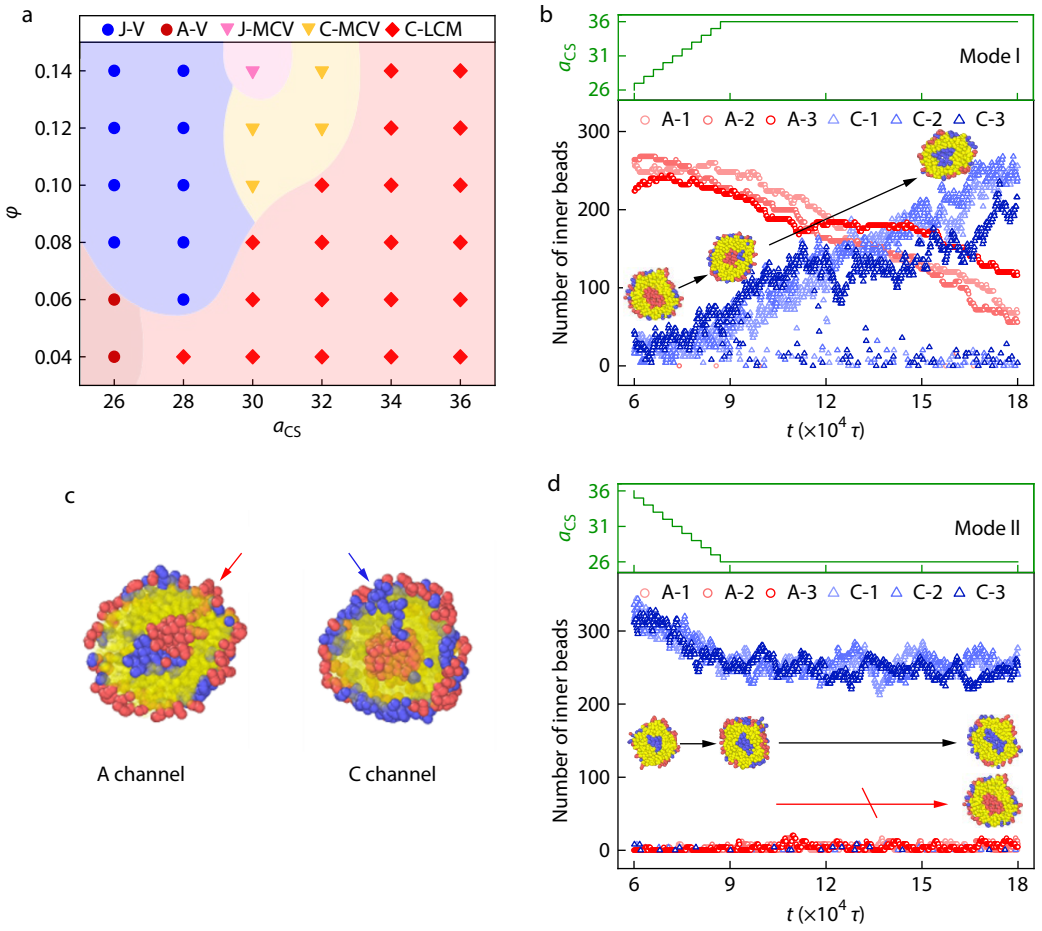

Fig. 4 (a) Morphological phase diagram of the co-assembled aggregates formed in terms of the interaction parameter a_{CS} and polymer concentration φ with a_{AC}=70, a_{AB}=70, a_{BC}=50, a_{AS}=30, a_{BS}=80, and φ_{AB}=φ_{BC}. Time evolution of the numbers of A and C beads located inside the aggregates under (b) mode I and (d) mode II from three parallel simulations. Mode I: initially, a_{CS}=26, after 6×10$^4\tau$, a_{CS} was increased by 1 every 3×10$^3\tau$ until it reached 36, then maintained for 9×10$^4\tau$. Mode II: initially, a_{CS}=36, after 6×10$^4\tau$, a_{CS} was decreased by 1 every 3×10^3 τ until it reached 26, then maintained for 9×10$^4\tau$. The insets represent the cross-sectional snapshots of initial state (6×10$^4\tau$), ramp-completed state (9×10$^4\tau$), and equilibrated state (18×10$^4\tau$), illustrating the transformation of internal composition of the aggregates during the process. All other parameters were set as follows: a_{AC}=70, a_{AB}=70, a_{BC}=50, a_{AS}=30, a_{BS}=80, and φ_{AB}=φ_{BC}=0.03. (c) A/C channel formed during the rearrangement process under mode I. The hydrophobic block B is rendered translucent for clarity and the arrows point to the channels.

gates, forming a central domain rather than distinct compartments. Nevertheless, for convenience and clarity, the structure is still referred to as C-LCM.

To probe the response of the aggregates to external stimuli, two modes of parameter modification were designed: mode I (initial a_{CS}=26) and mode II (initial a_{CS}=36). After equilibration for 6×10$^4\tau$ to obtain the initial morphologies (A-V or C-LCM), a_{CS} was varied stepwise over 3×10$^4\tau$ to reach the final values (36 for mode I and 26 for mode II). The systems were subsequently equilibrated for an additional 9×10^4 τ.

As discussed above, the increase in a_{CS} facilitates the migration of block C toward the interior of the aggregates. To quantify this process, we analyzed the temporal variation in the numbers of internally distributed A and C beads under mode I and mode II, respectively, as shown in Figs. 4(b) and 4(d). The results show that, under mode I, the dominant block within the aggregates undergoes an inversion, transitioning from block A to predominant block C. In contrast, under mode II, the aggregate interior is consistently dominated by block C. Under mode I, the inward migration of block C is governed by the coupled thermodynamic and kinetic effects. Relative to block A, the higher a_{CS} in combination with the lower a_{BC} provides a thermodynamic driving force for the relocation of block C toward the aggregate interior. The lower a_{BC} also corresponds to a lower free-energy barrier for transmembrane transport and higher mobility of block C. As a result, C blocks traverse the hydrophobic membrane, leading to an inversion of the dominant hydrophilic block within the aggregate. Video S1 (in ESI) displays the dynamic rearrangement of hydrophilic blocks observed in the simulation. Representative snapshots are shown in Fig. 4(c), corresponding to the state in Fig. 4(b), where the number of hydrophilic beads approaches zero, indicating connectivity between the inner and outer regions of the aggregate. For mode II, the "freezing" of the aggregate structure can be attributed to analogous thermodynamic and kinetic factors acting in the opposite direction. In the initial C-LCM, the absence of encapsulated solvent prevents the interior C blocks from interacting with the

https://doi.org/10.1007/s10118-026-3732-4

solvent, hindering their migration. At the same time, the lower a_{BC} thermodynamically favors the retention of block C within the aggregate. Moreover, due to the higher a_{AB}, the large unfavorable enthalpy of interaction with the hydrophobic layer formed by block B leads to the presence of kinetic traps, which restrict the inward migration of A blocks. Overall, the structural transition of the aggregates in response to external stimuli exhibits strong kinetic control over morphology inversion.

Control of the Inversion Process

The structural asymmetry of aggregates with a dominant single-block internal composition offers distinct advantages for biomedical applications, including precise drug loading, targeting, and efficient release.[54,55] The controlled inversion of the dominant block triggered by external stimuli enables precise tuning of the drug release process, allowing for either rapid or sustained release to meet specific therapeutic needs and enhance treatment efficacy. To elucidate the regulatory mechanisms underlying the rearrangement of hydrophilic blocks, we conducted an exploration by varying the initial interaction parameters.

Specifically, while keeping other interaction parameters constant, we either decreased the repulsion between blocks A and B (a_{AB}) or increased the repulsion between blocks C and B (a_{BC}), as shown in Fig. 5. The results show that when a_{AB} decreases from 70 to 40, the dominant internal block undergoes an inversion in both modes and equilibrium is reached more rapidly, as shown in Figs. 5(a) and 5(b). Under mode II, the lower a_{AB} reduces the energy barrier for block A to traverse the hydrophobic layer, enabling the stimulus-driven inward migration of A blocks. The reduced resistance encountered by block A when traversing the hydrophobic layer also enhances its mobility, which in turn accelerates the inversion process. In contrast, when a_{BC} increases from 50 to 80, the dominant internal block remains unchanged over the simulation time, as shown in Figs. 5(c) and 5(d). In this case, block C has difficulty in crossing the hydrophobic layer under both modes. These results further confirm the energy barrier effect of the hydrophobic layer on the inversion of the aggregates. The interactions between the hydrophilic and hydrophobic blocks regulate the response of the aggregate to external stimuli.

The intrinsic hydrophobicity of the hydrophobic layer also contributes to the energy barrier that blocks A and C must overcome during rearrangement.[41] To examine its influence on the dynamic process, the initial interaction parameter between the hydrophobic block B and the solvent (a_{BS}) was varied, as shown in Fig. 6. Figs. 6(a) and 6(b) demonstrate that, under mode I, decreasing a_{BS} accelerates the inversion process. At a_{BS}=50, equilibrium is reached at an earlier stage, with the dominant internal block transitioning from A to C. This behavior can be attributed to the reduced repulsion between block B and the solvent, which loosens the packing of

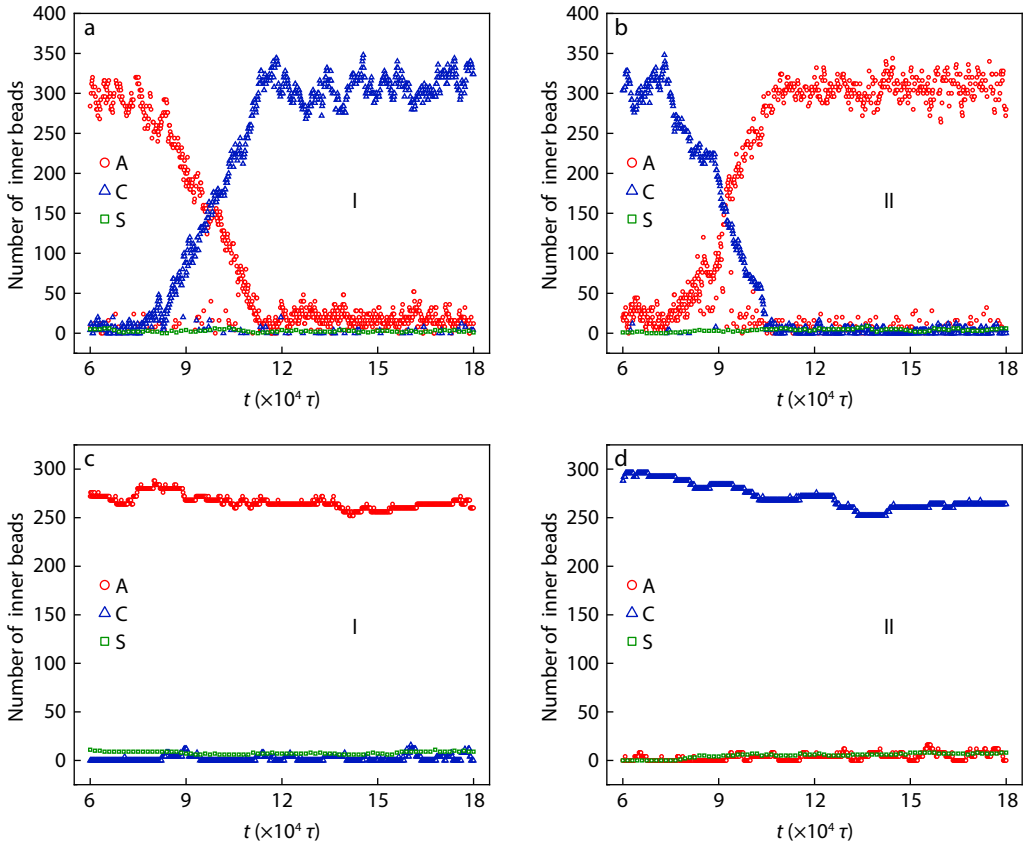

Fig. 5 Variations of the number of A, C, and S beads located inside the aggregates with time under (a) mode I or (b) mode II when a_{AB}=40 and a_{BC}=50. Variations of the number of A, C, and S beads located inside the aggregates with time under (c) mode I or (d) mode II when a_{AB}=70 and a_{BC}=80. Parameters were set: a_{AC}=70, a_{AS}=30, a_{BS}=80, and $\varphi_{AB}=\varphi_{BC}$=0.03.

https://doi.org/10.1007/s10118-026-3732-4

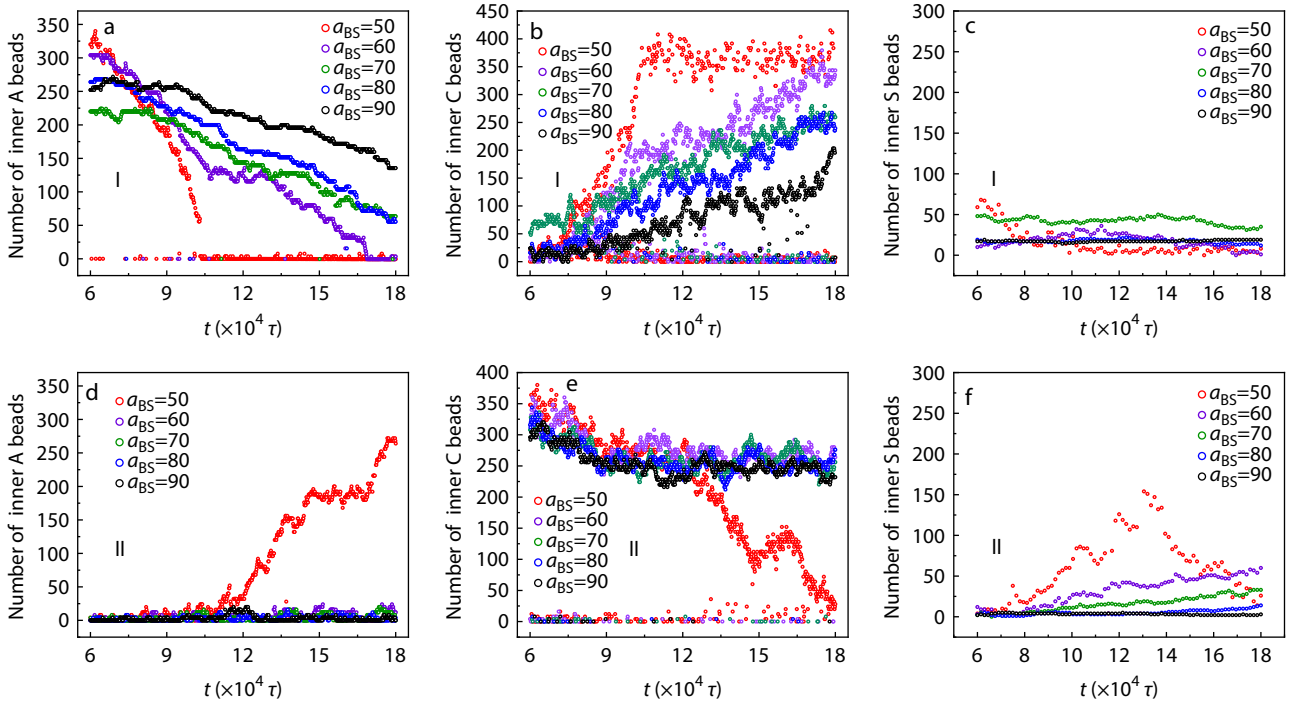

Fig. 6 (a–c) Variations of the number of (a) A, (b) C, and (c) S beads located inside the aggregates with time under mode I at different values of a_{BS}. (d–f) Variations of the number of (d) A, (e) C, and (f) S beads located inside the aggregates with time under mode II at different values of a_{BS}. Parameters were set: a_{AC}=70, a_{AB}=70, a_{BC}=50, a_{AS}=30, and φ_{AB}=φ_{BC}=0.03.

the hydrophobic layer, lowers the energy barrier for hydrophilic blocks to traverse the membrane, and facilitates their migration. In addition, as shown in Fig. 6(c), the number of solvent beads located inside the aggregate exhibits only minimal variation during the inversion process. Under mode II, when a_{BS} ranges from 60 to 90, the dominant internal block remains almost unchanged, as shown in Figs. 6(d) and 6(e). In contrast, a clear inversion phenomenon is observed at a_{BS}= 50. This indicates that a sufficiently low a_{BS} significantly weakens the barrier effect of the hydrophobic layer, thereby increasing membrane permeability and enabling migration of hydrophilic blocks. Another interesting finding is that, as shown in Fig. 6(f), as a_{BS} decreases, more solvent beads penetrate the aggregate, enhancing solvent contact with internally distributed C blocks, which alleviates the energetic strain caused by kinetic traps.

CONCLUSIONS

In conclusion, this study systematically investigates the co-assembly behavior and structural transitions of a binary mixture of AB/BC block copolymers in dilute solution. By modulating the interaction parameters, we elucidate their effects on aggregate morphology and characterize the phase separation of hydrophilic blocks A and C. We observed a variety of structures, including vesicles, multicompartment vesicles, and large compound micelles, with different patterns of internal distributions of blocks A and C. Furthermore, treating variations in the repulsion between the hydrophilic block C and the solvent (a_{CS}) as an external stimulus, two distinct dynamic modes (mode I and mode II) are established to examine the reversibility of the dominant block within the aggregates. The results indicate that the barrier effect of the hydrophobic layer restricts the rearrangement of the hydrophilic blocks, leading to kinetic traps and structural "freezing". By tuning the interaction parameters between the hydrophilic and hydrophobic blocks as well as between the hydrophobic block and the solvent, the mobility of the hydrophilic blocks and the barrier effect of the hydrophobic layer can be effectively regulated, thereby controlling the occurrence and kinetics of inversion. This mechanistic framework enables deliberate acceleration or deceleration of the inversion process and provides a means to "unfreeze" otherwise kinetically trapped aggregate structures. The controllable inversion of asymmetric aggregates revealed here establishes a theoretical foundation for the design of stimuli-responsive drug delivery systems, offering a pathway toward the advancement of controlled drug delivery and release technologies.

Conflict of Interests

The authors declare no interest conflict.

Electronic Supplementary Information

Electronic supplementary information (ESI), which includes details of the simulation method (Fig. S1 in ESI), morphology phase diagram of the pure AB system as a function of relative chain length and corresponding cluster analysis (Fig. S2 in ESI), morphological phase diagram of the aggregates formed by A_4B_9 diblock copolymers in terms of the interaction parameters a_{AB} and a_{BS} (Fig. S3 in ESI), snapshots of vesicle formation process *via* the bilayer membrane closure mechanism in the mixture (PDF); Video S1, the rearrangement process of hydrophilic blocks A

https://doi.org/10.1007/s10118-026-3732-4

and C from a cross-sectional view (AVI), is available free of charge in the online version of this article at https://doi.org/10.1007/s10118-026-3732-4.

Data Availability Statement

The data that support the findings of this study are available from the corresponding author upon reasonable request.

ACKNOWLEDGMENTS

This work was financially supported by the National Natural Science Foundation of China (Nos. 92477118, 52573024, and 22173045) and National Science and Technology Major Project (No. 2025ZD1407303). The numerical calculations have been done on the IBM Blade cluster system in the High Performance Computing Center (HPCC) of Nanjing University.

REFERENCES

1 Wong, C. K.; Qiang, X.; Müller, A. H. E.; Gröschel, A. H. Self-assembly of block copolymers into internally ordered microparticles. *Prog. Polym. Sci.* **2020**, *102*, 101211.
2 Xiao, J.; Du, J. Tetrapod polymersomes. *J. Am. Chem. Soc.* **2020**, *142*, 6569−6577.
3 Wong, C. K.; Heidelmann, M.; Dulle, M.; Qiang, X.; Förster, S.; Stenzel, M. H.; Gröschel, A. H. Vesicular polymer hexosomes exhibit topological defects. *J. Am. Chem. Soc.* **2020**, *142*, 10989−10995.
4 Zhang, L.; Yang, Z.; Xia, W.; Li, J.; Yang, H.; Yang, S.; Chen, E.-Q. Liquid crystal promoted self-assembly of statistical copolymers into diverse nanostructures with precise dimensions. *J. Am. Chem. Soc.* **2024**, *146*, 31221−31229.
5 Iqbal, S.; Blenner, M.; Alexander-Bryant, A.; Larsen, J. Polymersomes for therapeutic delivery of protein and nucleic acid macromolecules: from design to therapeutic applications. *Biomacromolecules* **2020**, *21*, 1327−1350.
6 Kayani, A.; Raza, A.; Si, J.; Dutta, D.; Zhou, Q.; Ge, Z. Polymersome membrane engineering with active targeting or controlled permeability for responsive drug delivery. *Biomacromolecules* **2023**, *24*, 4622−4645.
7 Putranto, A. F.; Fleury, G.; Wulandari, C.; Muslihati, A.; Amrillah, Y. T.; Yuliarto, B.; Kogelschatz, M.; Nugroho, F. A. A.; Wasisto, H. S.; Zelsmann, M. Block copolymer self-assembly for biological and chemical sensing. *ACS Appl. Polym. Mater.* **2024**, *6*, 14970−15001.
8 Li, C.; Li, Q.; Kaneti, Y. V.; Hou, D.; Yamauchi, Y.; Mai, Y. Self-assembly of block copolymers towards mesoporous materials for energy storage and conversion systems. *Chem. Soc. Rev.* **2020**, *49*, 4681−4736.
9 Cummins, C.; Lundy, R.; Walsh, J. J.; Ponsinet, V.; Fleury, G.; Morris, M. A. Enabling future nanomanufacturing through block copolymer self-assembly: a review. *Nano Today* **2020**, *35*, 100936.
10 Chen, Y.; Zhang, K.; Wang, X.; Zhang, F.; Zhu, J.; Mays, J. W.; Wooley, K. L.; Pochan, D. J. Multigeometry nanoparticles: hybrid vesicle/cylinder nanoparticles constructed with block copolymer solution assembly and kinetic control. *Macromolecules* **2015**, *48*, 5621−5631.
11 Xu, J.; Wang, K.; Liang, R.; Yang, Y.; Zhou, H.; Xie, X.; Zhu, J. Structural transformation of diblock copolymer/homopolymer assemblies by tuning cylindrical confinement and interfacial interactions. *Langmuir* **2015**, *31*, 12354−12361.
12 Zhang, Z.; Ma, R.; Shi, L. Cooperative macromolecular self-assembly toward polymeric assemblies with multiple and bioactive functions. *Acc. Chem. Res.* **2014**, *47*, 1426−1437.
13 Ebrahim Attia, A. B.; Ong, Z. Y.; Hedrick, J. L.; Lee, P. P.; Ee, P. L. R.; Hammond, P. T.; Yang, Y. Y. Mixed micelles self-assembled from block copolymers for drug delivery. *Curr. Opin. Colloid Interface Sci.* **2011**, *16*, 182−194.
14 Gerardos, A. M.; Balafouti, A.; Pispas, S. Mixed copolymer micelles

Graphical Abstract

Morphology Inversion Induced by Stimuli-responsive Blocks in the AB/BC Block Copolymer Assemblies in Solution

Zi-Xuan Zhang, Hao Tang, Xian-Deng Qiu, Yuan Li, Mao-Zhang Tian, and Rong Wang

Nanjing University; PetroChina Research Institute of Petroleum Exploration & Development; State Key Laboratory of Enhanced Oil and Gas Recovery

Using DPD simulations, we revealed a kinetic-control mechanism governing the inversion of the dominant internal block in AB/BC co-assemblies under external stimuli. The occurrence and kinetics of inversion are controlled by adjusting key interaction parameters that influence the mobility of the hydrophilic blocks and the barrier effect of the hydrophobic layer.

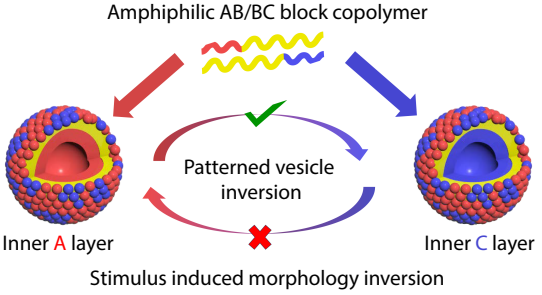

Chinese J. Polym. Sci., 2026 *https://doi.org/10.1007/s10118-026-3732-4*

for nanomedicine. *Nanomanufacturing* **2023**, *3*, 233–247.
15 Yu, H.; Qiu, X.; Moreno, N.; Ma, Z.; Calo, V. M.; Nunes, S. P.; Peinemann, K.-V. Self-assembled asymmetric block copolymer membranes: bridging the gap from ultra- to nanofiltration. *Angew. Chem. Int. Ed.* **2015**, *54*, 13937–13941.
16 Radjabian, M.; Abetz, V. Tailored pore sizes in integral asymmetric membranes formed by blends of block copolymers. *Adv. Mater.* **2015**, *27*, 352–355.
17 Sproncken, C. C. M.; Liu, P.; Monney, J.; Fall, W. S.; Pierucci, C.; Scholten, P. B. V.; Van Bueren, B.; Penedo, M.; Fantner, G. E.; Wensink, H. H.; Steiner, U.; Weder, C.; Bruns, N.; Mayer, M.; Ianiro, A. Large-area, self-healing block copolymer membranes for energy conversion. *Nature* **2024**, *630*, 866–871.
18 Liu, G.; Ma, R.; Ren, J.; Li, Z.; Zhang, H.; Zhang, Z.; An, Y.; Shi, L. A glucose-responsive complex polymeric micelle enabling repeated on–off release and insulin protection. *Soft Matter* **2013**, *9*, 1636–1644.
19 Hespel, L.; Asmar, A. E.; Morandi, G.; Lecamp, L.; Picton, L.; Burel, F. Synthesis of dual-sensitive core cross-linked mixed micelles through thiol–ene addition and subsequent drug release behavior. *Macromol. Chem. Phys.* **2017**, *218*, 1700016.
20 Chien, Y. Y.; Wang, T. Y.; Liao, P. W.; Wu, W. C.; Chen, C. Y. Folate-conjugated and dual stimuli-responsive mixed micelles loading indocyanine green for photothermal and photodynamic therapy. *Macromol. Biosci.* **2018**, *18*, 1700409.
21 Li, K.; Zang, X.; Meng, X.; Li, Y.; Xie, Y.; Chen, X. Targeted delivery of quercetin by biotinylated mixed micelles for non-small cell lung cancer treatment. *Drug Deliv.* **2022**, *29*, 970–985.
22 Sui, Y.; Li, J.; Qu, J.; Fang, T.; Zhang, H.; Zhang, J.; Wang, Z.; Xia, M.; Dai, Y.; Wang, D. Dual-responsive nanovaccine for cytosolic delivery of antigens to boost cellular immune responses and cancer immunotherapy. *Asian J. Pharm. Sci.* **2022**, *17*, 583–595.
23 Kim, T. H.; Mount, C. W.; Dulken, B. W.; Ramos, J.; Fu, C. J.; Khant, H. A.; Chiu, W.; Gombotz, W. R.; Pun, S. H. Filamentous, mixed micelles of triblock copolymers enhance tumor localization of indocyanine green in a murine xenograft model. *Mol. Pharm.* **2012**, *9*, 135–143.
24 Zhu, J.; Zhang, S.; Zhang, K.; Wang, X.; Mays, J. W.; Wooley, K. L.; Pochan, D. J. Disk-cylinder and disk-sphere nanoparticles via a block copolymer blend solution construction. *Nat. Commun.* **2013**, *4*, 2297.
25 Yue, X.; Geng, Z.; Yan, N.; Jiang, W. Hierarchical self-assembly of a PS-b-P4VP/PS-b-PNIPAM mixture into multicompartment micelles and their response to two-dimensional confinement. *Phys. Chem. Chem. Phys.* **2020**, *22*, 1194–1203.
26 Ryu, M.-C.; Choi, S.-H. Influence of polymer architecture on the structure of complex coacervate core micelles: AB + AC versus AB + C systems. *ACS Macro Lett.* **2025**, *14*, 2–7.
27 Christian, D. A.; Tian, A.; Ellenbroek, W. G.; Levental, I.; Rajagopal, K.; Janmey, P. A.; Liu, A. J.; Baumgart, T.; Discher, D. E. Spotted vesicles, striped micelles and janus assemblies induced by ligand binding. *Nat. Mater.* **2009**, *8*, 843–849.
28 Hu, J.; Liu, G. Chain mixing and segregation in B–C and C–D diblock copolymer micelles. *Macromolecules* **2005**, *38*, 8058–8065.
29 Palanisamy, A.; Guo, Q. Large compound vesicles from amphiphilic block copolymer/rigid-rod conjugated polymer complexes. *J. Phys. Chem. B* **2014**, *118*, 12796–12803.
30 Luo, L.; Eisenberg, A. One-step preparation of block copolymer vesicles with preferentially segregated acidic and basic corona chains. *Angew. Chem. Int. Ed.* **2002**, *41*, 1001–1004.
31 Vyhnalkova, R.; Müller, A. H. E.; Eisenberg, A. Control of corona composition and morphology in aggregates of mixtures of PS-b-PAA and PS-b-P4VP diblock copolymers: effects of pH and block length. *Langmuir* **2014**, *30*, 5031–5040.
32 Vyhnalkova, R.; Müller, A. H. E.; Eisenberg, A. Control of morphology and corona composition in aggregates of mixtures of PS-b-PAA and PS-b-P4VP diblock copolymers: effects of solvent, water content, and mixture composition. *Langmuir* **2014**, *30*, 13152–13163.
33 Zhu, J.; Zhang, S.; Zhang, F.; Wooley, K. L.; Pochan, D. J. Hierarchical assembly of complex block copolymer nanoparticles into multicompartment superstructures through tunable interparticle associations. *Adv. Funct. Mater.* **2013**, *23*, 1767–1773.
34 Zhou, J.; Tang, H.; Wang, R. Co-assembly of amphiphilic triblock copolymers with nanodrugs and drug release kinetics in solution. *J. Phys. Chem. B* **2024**, *128*, 2841–2852.
35 Li, S.; Yu, C.; Zhou, Y. Phase diagrams, mechanisms and unique characteristics of alternating-structured polymer self-assembly via simulations. *Sci. China Chem.* **2019**, *62*, 226–237.
36 Guo, W. X.; Hu, L. F.; Feng, Y. H.; Chen, B. Z.; Guo, X. D. Advances in self-assembling of pH-sensitive polymers: a mini review on dissipative particle dynamics. *Colloids Surf. B Biointerfaces* **2022**, *210*, 112202.
37 Tang, H.; Qiu, X.; Xie, D.; Wang, R. Templated fabrication of DNA-programmable vesicles via amphiphile-functionalized nanoparticles. *Macromolecules* **2025**, *58*, 3082–3091.
38 Bai, J.-L.; Liu, D.; Wang, R. Self-assembly of amphiphilic diblock copolymers induced by liquid-liquid phase separation. *Chinese J. Polym. Sci.* **2021**, *39*, 1217–1224.
39 Wang, Z.; Wang, H.; Cheng, M.; Li, C.; Faller, R.; Sun, S.; Hu, S. Controllable multigeometry nanoparticles via cooperative assembly of amphiphilic diblock copolymer blends with asymmetric architectures. *ACS Nano* **2018**, *12*, 1413–1419.
40 Liu, F.; Eisenberg, A. Preparation and pH triggered inversion of vesicles from poly(acrylic acid)-block-polystyrene-block-poly(4-vinyl pyridine). *J. Am. Chem. Soc.* **2003**, *125*, 15059–15064.
41 Geng, Z.; Han, Y.; Jiang, W. Structural transformation of vesicles formed by a polystyrene-b-poly(acrylic acid)/polystyrene-b-poly(4-vinyl pyridine) mixture: from symmetric to asymmetric membranes. *Soft Matter* **2017**, *13*, 2634–2642.
42 Jin, Q.; Liu, G.; Ji, J. Micelles and reverse micelles with a photo and thermo double-responsive block copolymer. *J. Polym. Sci. Part Polym. Chem.* **2010**, *48*, 2855–2861.
43 Morrison, C. A.; Chan, E. P.; Deming, T. J. Triggered inversion of dual responsive diblock copolypeptide vesicles. *J. Am. Chem. Soc.* **2025**, *147*, 7617–7623.
44 Hoogerbrugge, P. J.; Koelman, J. M. V. A. Simulating microscopic hydrodynamic phenomena with dissipative particle dynamics. *Europhys. Lett.* **1992**, *19*, 155.
45 Feng, Y. H.; Zhang, X. P.; Zhao, Z. Q.; Guo, X. D. Dissipative particle dynamics aided design of drug delivery systems: a review. *Mol. Pharm.* **2020**, *17*, 1778–1799.
46 Yang, J.; Wang, R.; Xie, D. Aqueous self-assembly of amphiphilic cyclic brush block copolymers as asymmetry-tunable building blocks. *Macromolecules* **2019**, *52*, 7042–7051.
47 Groot, R. D.; Warren, P. B. Dissipative particle dynamics: bridging the gap between atomistic and mesoscopic simulation. *J. Chem. Phys.* **1997**, *107*, 4423–4435.
48 Thompson, A. P.; Aktulga, H. M.; Berger, R.; Bolintineanu, D. S.; Brown, W. M.; Crozier, P. S.; in 't Veld, P. J.; Kohlmeyer, A.; Moore, S. G.; Nguyen, T. D.; Shan, R.; Stevens, M. J.; Tranchida, J.; Trott, C.; Plimpton, S. J. LAMMPS—a flexible simulation tool for particle-

based materials modeling at the atomic, meso, and continuum scales. *Comput. Phys. Commun.* **2022**, *271*, 108171.
49 Stukowski, A. Visualization and analysis of atomistic simulation data with ovito–the open visualization tool. *Model. Simul. Mater. Sci. Eng.* **2010**, *18*, 015012.
50 Cui, J.; Han, Y.; Jiang, W. Asymmetric vesicle constructed by AB/CB diblock copolymer mixture and its behavior: a monte carlo study. *Langmuir* **2014**, *30*, 9219−9227.
51 Du, K. Copolymers induced co-assembly for constructing novel micellar carriers by computer simulations. *Chem. Phys. Lett.* **2022**, *803*, 139874.
52 Luo, L.; Eisenberg, A. Thermodynamic stabilization mechanism of block copolymer vesicles. *J. Am. Chem. Soc.* **2001**, *123*, 1012−1013.
53 Wang, Y.; Lin, M.; Fan, T.; Zhou, M.; Yin, R.; Wang, X. Advances of stimuli-responsive amphiphilic copolymer micelles in tumor therapy. *Int. J. Nanomed.* **2025**, *20*, 1−24.
54 Huang, P.; Qi, M.; Chen, C.; Xu, F.; Li, S.; Xu, Q.; Pan, H.; Wang, Y.; Yu, C.; Zhang, S.; Zhou, Y. Asymmetric vesicles self-assembled by amphiphilic sequence-controlled polymers. *ACS Macro Lett.* **2021**, *10*, 894−900.
55 Daubian, D.; Fillion, A.; Gaitzsch, J.; Meier, W. One-pot synthesis of an amphiphilic ABC triblock copolymer PEO-b-PEHOx-b-PEtOz and its self-assembly into nanoscopic asymmetric polymersomes. *Macromolecules* **2020**, *53*, 11040−11050.

https://doi.org/10.1007/s10118-026-3732-4